AIAA SciTech Forum
7-11 January 2019, San Diego, California
AIAA Scitech 2019 Forum

10.2514/6.2019-0589

Design of Injection Jet Span Profile for Co-Flow Jet Airfoil

Yan Ren * Gecheng Zha †
Dept. of Mechanical and Aerospace Engineering
University of Miami, Coral Gables, Florida 33124
E-mail: gzha@miami.edu

Abstract

This paper presents the design of injection duct span width distribution of co-flow jet (CFJ) flow control airfoils in cruise condition. The duct cross section outlines are mathematically modeled as superellipse, which has a parameter η to control the outline shape. The semi major axis of the superellipse, which controls the span profile of the jet, is of great importance to the overall performance of the duct and the CFJ airfoil. The aerodynamic performance of the ducts are evaluated via numerical simulations, which employ 3D RANS solver with Spalart-Allmaras (S-A) turbulence model, 3th order WENO scheme for the inviscid fluxes, and 2nd order central differencing for the viscous terms. The duct inlet shape is predetermined according to the micro-compressor performance, and the associated boundary conditions are configured based on the 2D simulation results of CFJ airfoils and micro-compressors. The design goal is to eliminate flow separation, maximize the total pressure recovery, and minimize the spanwise velocity at the injection duct outlet.

The simulation results show that the duct span width distribution is crucial to control the spanwise velocity at the duct outlet. Smaller span over diameter ratio (W/D) leads to much smaller deviation angle (β) of the flow at the outlet. Moreover, a diverging-converging distribution of the duct span width leads to even smaller β angle. However, such profiles are more likely to cause flow separation at the two ends of the duct in spanwise direction. In the current study, the duct with $W/D = 6.5$ (design a) shows 95% total pressure recovery, while the duct with $W/D = 5$ (design b) shows 96.4% total pressure recovery. The first duct with diverging-converging duct span width distribution (design c) presents only half of the maximum β angle comparing to design b, but the total pressure recovery is a little bit lower (95.8%) due to flow separation at the two ends of the duct in spanwise direction. The second duct with diverging-converging duct span width distribution (design d) presents 85% of the maximum β angle comparing to design b, and the total pressure recovery is almost the same (96.3%) since the flow separation at the two ends of the design c in spanwise direction are removed. The aerodynamic performance of design d is the best in terms of low spanwise velocity and high total pressure recovery.

Nomenclature

SD	Suction duct
ID	Injection duct
AFC	Active Flow Control
CFJ	Co-Flow Jet
LE	Leading edge
TE	Trailing edge

* Postdoc Researcher, Ph.D., AIAA member
† Professor, ASME Fellow, AIAA associate Fellow

$FASIP$	Flow-Acoustics-Structure Interaction Package
$RANS$	Reynolds-Averaged Navier-Stokes
$ZNMF$	Zero-Net Mass Flux
η	Superellipse shape parameter
β	Deviation angle
P_{tr}	Total pressure ratio
M	Mach number
Γ	Gamma function
ρ	Density
V	Velocity
P_{01}	Total pressure at the inlet
P_{02}	Total pressure at the outlet
$\dot{m}$	Mass flow rate
$_\infty$	Subscript, stands for free stream
$_{cs}$	Subscript, stands for cross section
$_i$	Subscript, stands for inlet
$_o$	Subscript, stands for outlet

1 Introduction

In the past three decades, Active Flow Control (AFC) has attracted lots of interests as a means to enhance the performance of airfoil, which otherwise has appeared to be saturated based on conventional airfoil shape optimization. Co-Flow Jet (CFJ) airfoil is a zero-net mass-flux (ZNMF) flow control method recently developed by Zha et al. [1, 2, 3, 4, 5, 6, 7, 8, 9, 10, 11]. It is demonstrated to achieve radical lift augmentation, stall margin increase, drag reduction and moderate nose-down moment increase for stationary and pitching airfoils.

In the CFJ airfoil concept, an injection slot near the leading edge (LE) and a suction slot near the trailing edge (TE) on the airfoil suction surface are created. As shown in Fig. 1, a small amount of mass flow is withdrawn into the suction duct, pressurized and energized by a micro-compressor, and then injected near the LE tangentially to the main flow via an injection duct. The whole process does not add any mass flow to the system and hence is a ZNMF flow control. The flow inside the airfoil (in the suction and injection ducts) are essential to the overall CFJ airfoil performance. Any flow separations within the ducts will increase the energy expenditure. The injection duct is more challenging to design than the suction duct because the flow existing from the compressor always has some swirl angle. The flow at the injection duct is prone to flow separation and the jet tends to have spanwise velocity, which is not desirable for the flow control.

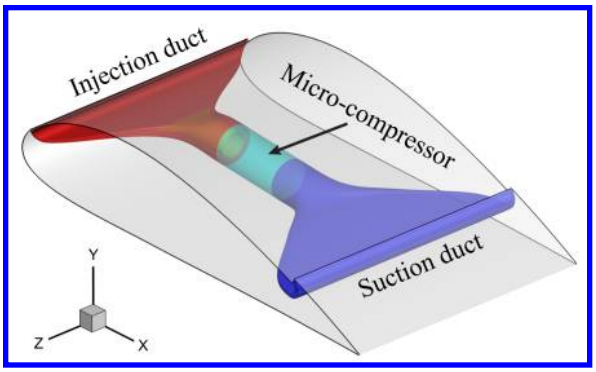

Figure 1: Schematic plot of a typical CFJ airfoil.

The purpose of this paper is to conduct the design of injection duct span width distribution in cruise condition. The suction duct is connected to the micro-compressor actuator inlet and the injection duct is connected to the micro-compressor outlet. In the current designs, the injection duct inlet size and location are predetermined by the 2D CFJ airfoil designs, so are the associated boundary conditions. The boundary conditions of the micro-compressor are determined by the design of the micro-compressor that meets the CFJ airfoil mass flow and pressure ratio requirements. The injection duct inlet is directly connected to the outlet of the micro-compressor, which presents a ring shape outline and generates swirl flow. In order to remove flow separation, a center body connecting to the inner circle of the micro-compressor outlet is used to guide the flow.

The requirements of the duct design are that there is no flow separation with uniform velocity distribution in spanwise and the pressure recovery is as high as possible. Moreover, small flow deviation angle (β) at the injection duct outlet is desirable.

2 Methodology

2.1 Duct Geometry

As shown in Fig. 1, the duct inlet and outlet have different shapes. The inlet of suction duct and outlet of injection duct have rectangular shape, whereas the outlet of suction duct and inlet of injection duct have circular shape. The method of calculating circular-to-rectangular transition surfaces developed in [12] is adopted.

A circle, an ellipse, and a rectangle are all specific cases of superellipses. The locus of points which make up a superellipse is defined as:

$$(\frac{y}{a})^{\eta} + (\frac{z}{b})^{\eta} = 1 \tag{1}$$

where a and b are semi major and minor axis of the superellipse. a and b are also the half width and half height of the duct cross section. η is shape parameter which controls the superellipse shape. The area enclosed by the superellipse A_{cs} can be computed as follows [13]:

$$A_{cs} = \frac{\Gamma(1/\eta)^2 4ab}{(\Gamma(2/\eta)2\eta)} \tag{2}$$

where Γ refers to the "gamma function" and is defined as:

$$\Gamma(\eta) = \int_0^\infty (e^{-t} t^{\eta-1}) dt \quad (\eta > 0) \tag{3}$$

With A_{cs}, a and b defined as continuous analytic functions of x (axis distance from the entrance), the transition surface is determined by iteratively computing $\eta(x)$ from Eq. (1). For practical applications, a rectangle ($\eta = \infty$) is accurately approximated with $\eta \geq 50$. In this paper, $\eta = 100$ is used to represent a rectangle.

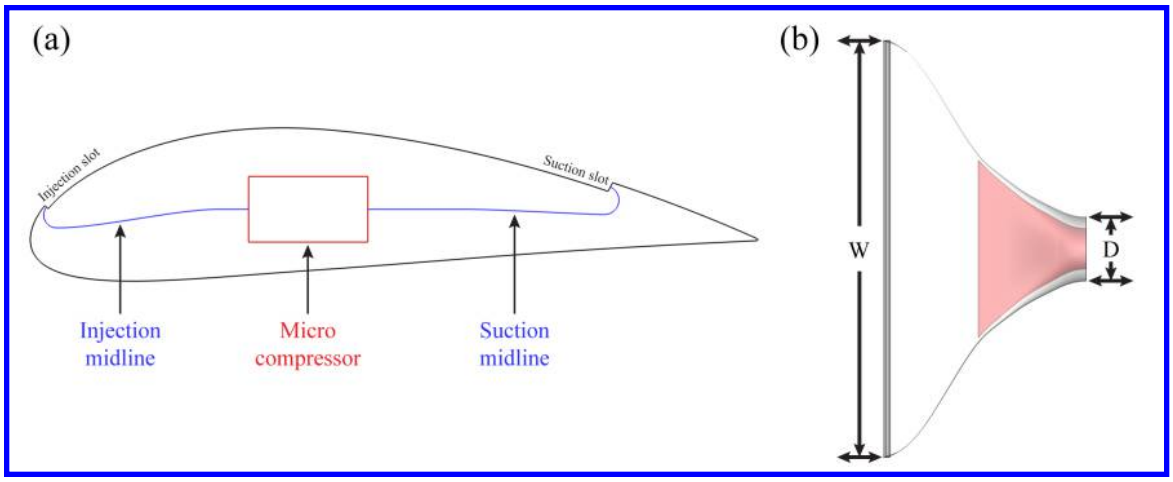

Figure 2: (a) CFJ airfoil configuration in cruise condition; (b) Definition of the duct W and D. The airfoil used here is CFJ-NACA 6421.

As shown in Fig. 2 (a), the CFJ airfoil injection and suction slot dimensions and locations are determined according to our previous published 2D design [14]. The injection and suction duct meanlines are determined based on the slot locations (blue curves in Fig. 2). We create superellipses along those duct meanlines, which pass through the superellipse geometric centers and locally perpendicular to the superellipses. The duct surfaces are formed by connecting those superellipses. Based on above mathematical model and geometry configuration, we successfully parameterize the problem, which is essential to the designs of the CFJ injection and suction ducts. In addition, the duct span over the diameter of the micro compressor outlet (W/D, Fig. 2 b) is a key parameter to study in this paper. It will greatly influence the duct performance.

2.2 Total Pressure Recovery

The best way of evaluating performance of a given duct is to calculate the total pressure recovery, which is defined as follows:

$$P_{tr} = \frac{\oiint_{S_o} \rho \mathbf{V} P_{02} d\mathbf{A}}{\oiint_{S_i} \rho \mathbf{V} P_{01} d\mathbf{A}} \tag{4}$$

where S_o and S_i stand the cross section interface at the inlet and outlet, respectively. P_{02} and P_{01} are the total pressure evaluated at outlet and inlet. The total pressure recovery P_{tr} is basically the mass averaged total pressure

ratio of outlet cross section and inlet cross section.

2.3 CFD Simulation Setup

The FASIP (Flow-Acoustics-Structure Interaction Package) CFD code is used to conduct the numerical simulation. The 3D Reynolds Averaged Navier-Stokes (RANS) equations with one-equation Spalart-Allmaras [15] turbulence model is used. A 3rd order WENO scheme for the inviscid flux [16, 17, 18, 19, 20, 21] and a 2nd order central differencing for the viscous terms [16, 20] are employed to discretize the Navier-Stokes equations. The low diffusion E-CUSP scheme used as the approximate Riemann solver suggested by Zha et al [17] is utilized with the WENO scheme to evaluate the inviscid fluxes. Implicit time marching method using Gauss-Seidel line relaxation is used to achieve a fast convergence rate [22]. Parallel computing is implemented to save wall clock simulation time [23].

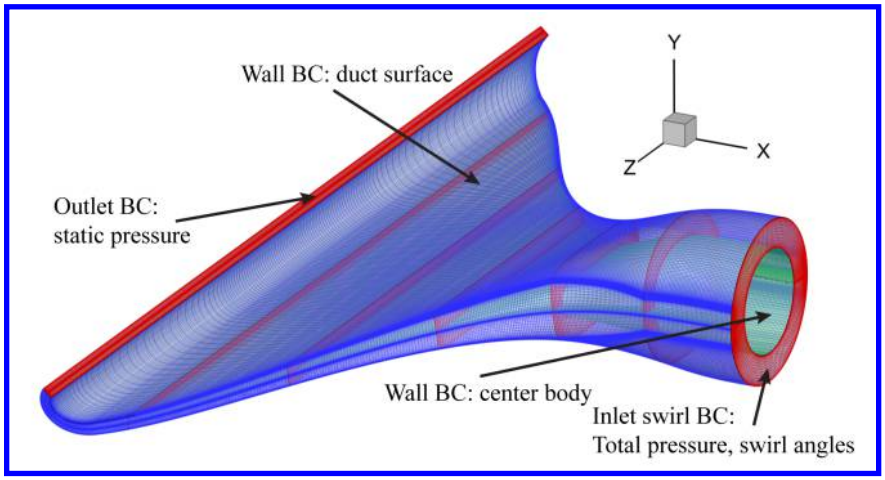

Figure 3: Computational mesh of injection duct in cruise condition.

The 3rd order accuracy no slip condition is enforced on the solid surface with the wall treatment suggested in [24] to achieve the flux conservation on the wall. As shown in Fig. 3, total pressure, total temperature and flow angles are specified at the duct inlet as boundary conditions. Static pressure is specified at the duct outlets as boundary conditions. The specific boundary conditions are based on the design of 2D CFJ airfoils [14] and micro-compressors [25]. The cross section faces of the ducts are meshed using "H" topology. Three hundreds points are placed in the streamwise direction, 60 points and 180 points are placed in the radial and circumferential direction. The total mesh size is 3.24 millions points, split into 12 blocks for the parallel computation. The first grid point on the duct surface is placed at $y^+ \approx 1$.

3 Results

Four different designs of the injection duct are discussed in this section: (a) $W/D = 6.5$; (b) $W/D = 5$; (c) and (d) $W/D = 5$ with two different diverging-converging duct span width distributions. Fig. 4 (a), (b), (c) and (d) show the geometries of the four designs, and Fig. 4 (e) and (f) show the streamwise duct span width (parameter a in Eq. (1)) and cross-section area distributions of those designs. As we can see in the figures, the duct span width distribution of design a and b are similar in shape but different in end values. The duct span width distribution

of design c and d show small peaks near $S = 0.7$ and $S = 0.9$, respectively, and then gradually decreases. They are two typical diverging-converging duct span width distributions. As shown in Fig. 4 (f), the cross-section areas of those designs gradually decrease while $S < 0.5$ (center body region), and keep constant afterwards. The cross-section area profile for the design b and d are overlapped.

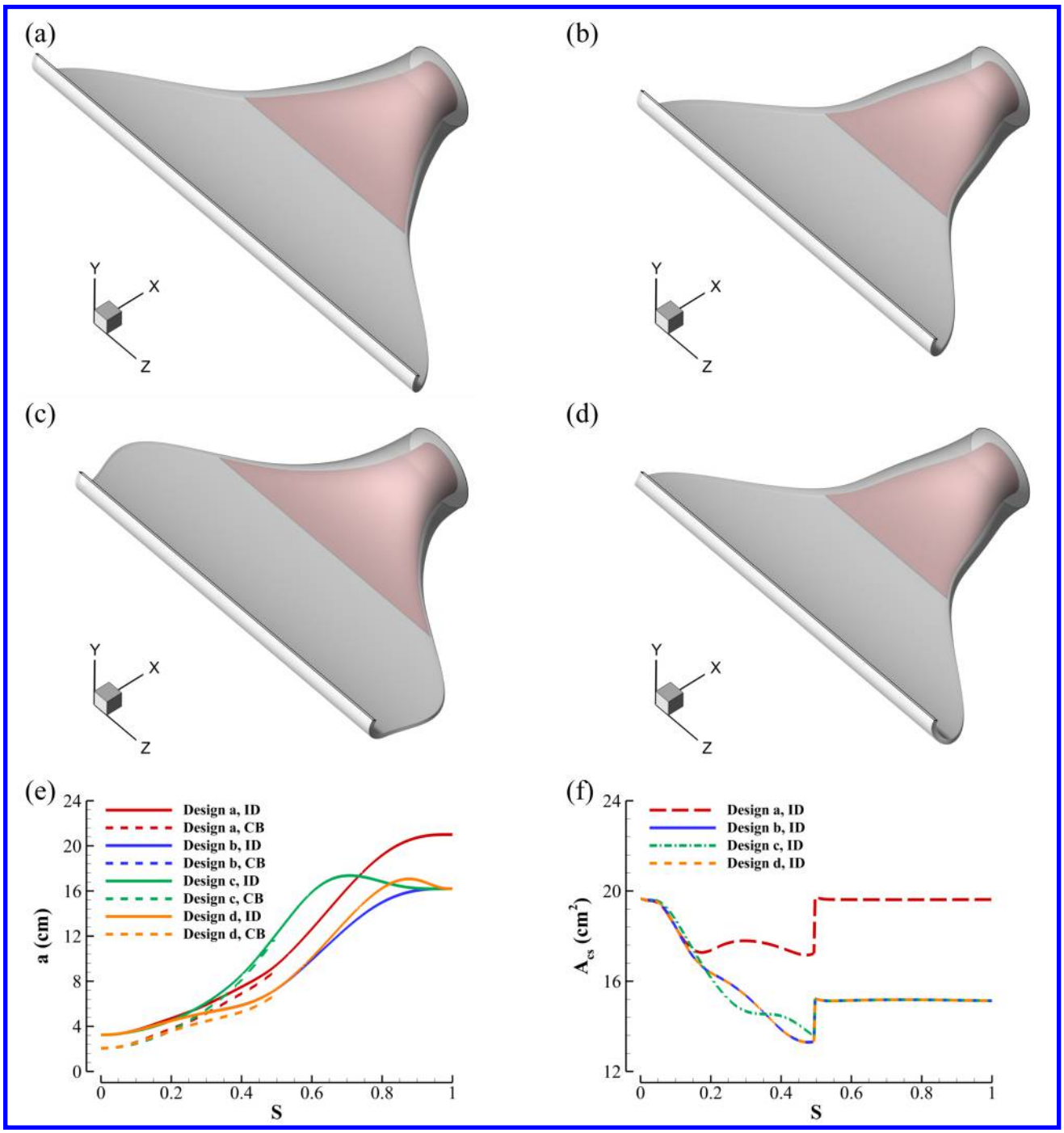

Figure 4: Injection duct span width (a) distribution with the duct centerline distance (S) from inlet to outlet (0 to 1): (a) design a; (b) design b; (c) design c; (d) design d.

Next, we look at the 3D streamlines (colored by Mach number) of the four cases. The results are plotted in Fig. 5. We can see that there are strong swirl flow directly coming out of the micro-compressor of those cases. The flow at the two sides of the center body has higher velocity and at the top and bottom surface of the center body has lower velocity. The center body is crucial to guide the flow. The flow has no separation for the design a, b and d. For design c, the flow at the two ends of the duct in spanwise direction is weak.

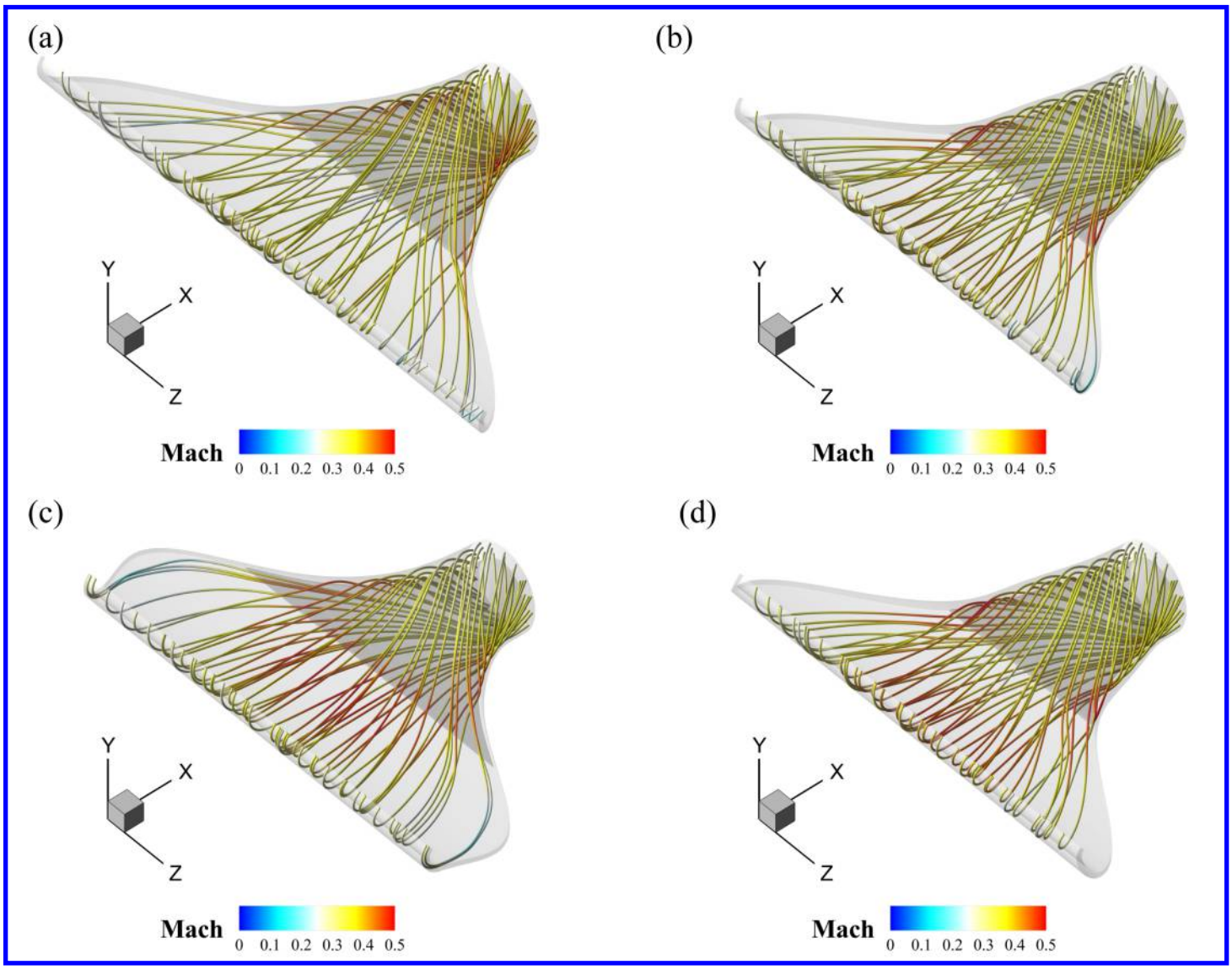

Figure 5: Simulated 3D streamlines inside the injection ducts. Colored by Mach number. (a) Design a; (b) design b; (c) design c; (d) design d.

Fig. 6 shows the 2D flow slices along z-direction (colored by Mach number). We can see in Fig. 6 that the flow is stronger near the two sides of the center body, which is due to the acceleration of the swirl flow when it's passing though the thin edge of the center body. That's why the center body *a* profile is crucial, and any improper profiles will lead to large flow separation around the edges of the center body. For design c, the two slices at the two ends of the duct in spanwise direction show weak flow, which may cause flow separation.

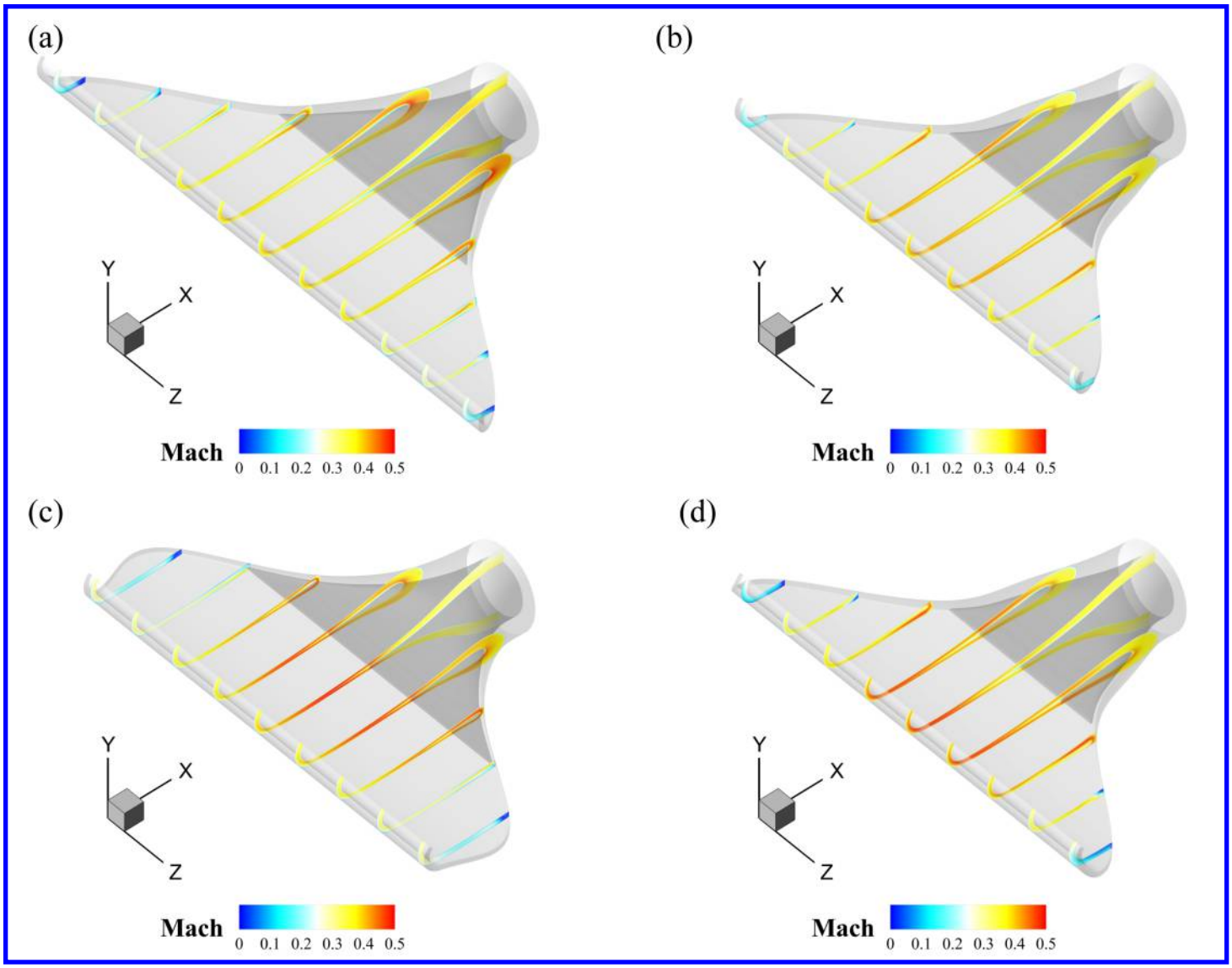

Figure 6: 2D flow slices in Z-direction, Colored by Mach number. (a) Design a; (b) design b; (c) design c; (d) design d.

We further cut flow slices through the meanline of the ducts, and the results are plotted in Fig. 7. The 2D streamlines are also plotted on the slices. For design a and b, we can see that the flow is very health. No flow separation can be observed. For design c, two large flow separations can be identified at the two ends of the duct in spanwise direction, which are caused by the rapid diverging of the duct span width distribution near $s = 0.7$. For design d, the diverging of the duct span width distribution is reduced and located more closer to the outlet of the duct. No flow separation can be identified in this design, although the flow is weaker near the diverging region comparing to design b.

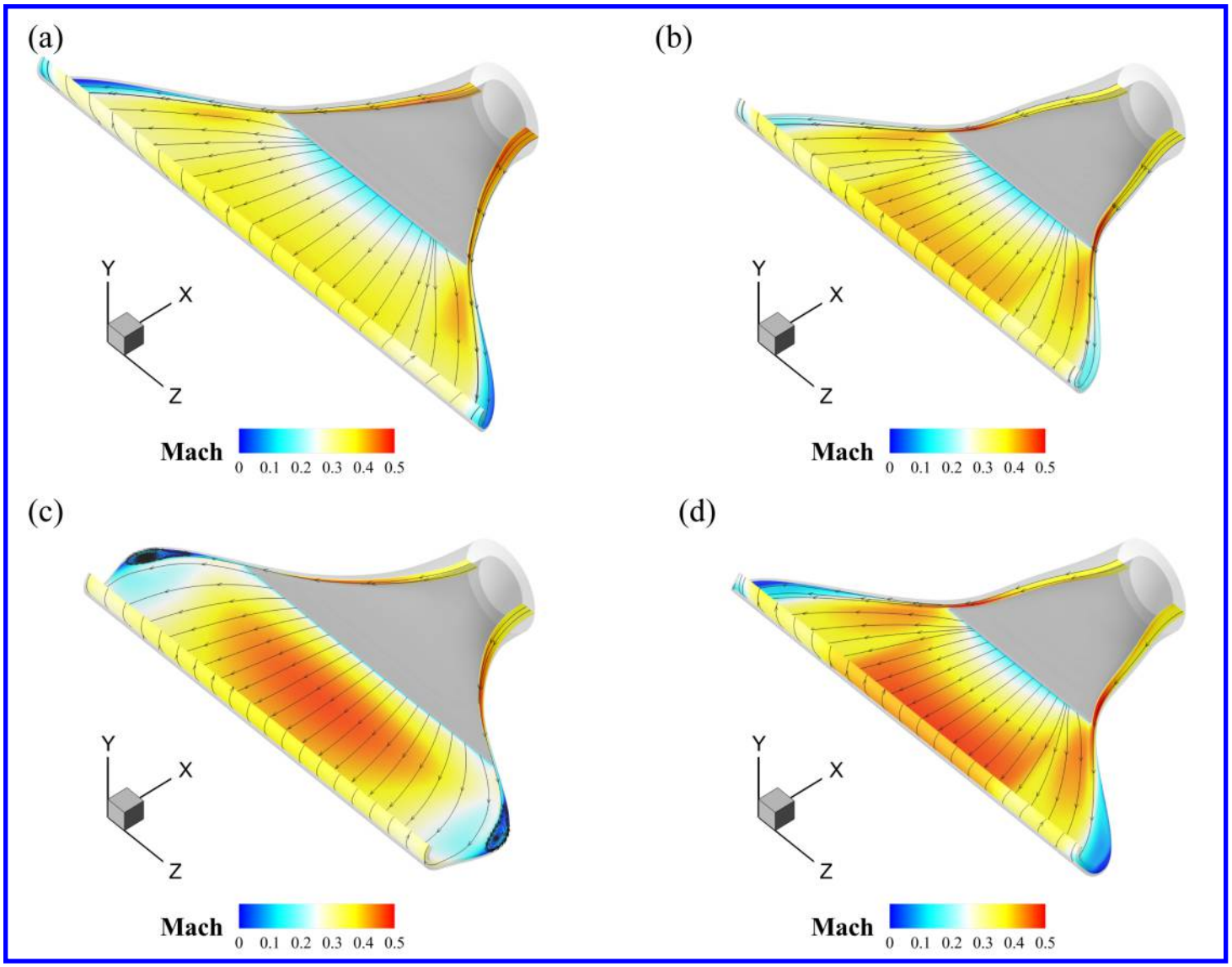

Figure 7: 2D flow slices through the meanline of the ducts, Colored by Mach number. (a) Design a; (b) design b; (c) design c; (d) design d.

Fig. 8 (a), (b), (c), and (d) show the total pressure contours on 2D flow slices along stream wise direction. As expected, the total pressure keeps decreasing along the duct for all cases. Fig. 8 (e) shows the mass flow averaged total pressure distribution along the stream wise direction for the three cases. We can see that the duct with $W/D = 6.5$ (design a) shows 95% total pressure recovery, while the duct with $W/D = 5$ (design b) shows 96.4% total pressure recovery. The first duct with diverging-converging duct span width distribution (design c) presents only half of the maximum β angle (flow deviation angle $\beta = atan(w/\sqrt{u^2 + v^2})$) comparing to design b, but the total pressure recovery is a little bit lower (95.8%) due to flow separation at the two ends of the duct in spanwise direction. The second duct with diverging-converging duct span width distribution (design d) presents 85% of the maximum β angle comparing to design b, and the total pressure recovery is almost the same (96.3%) since the flow separation at the two ends of the design c in spanwise direction are removed.

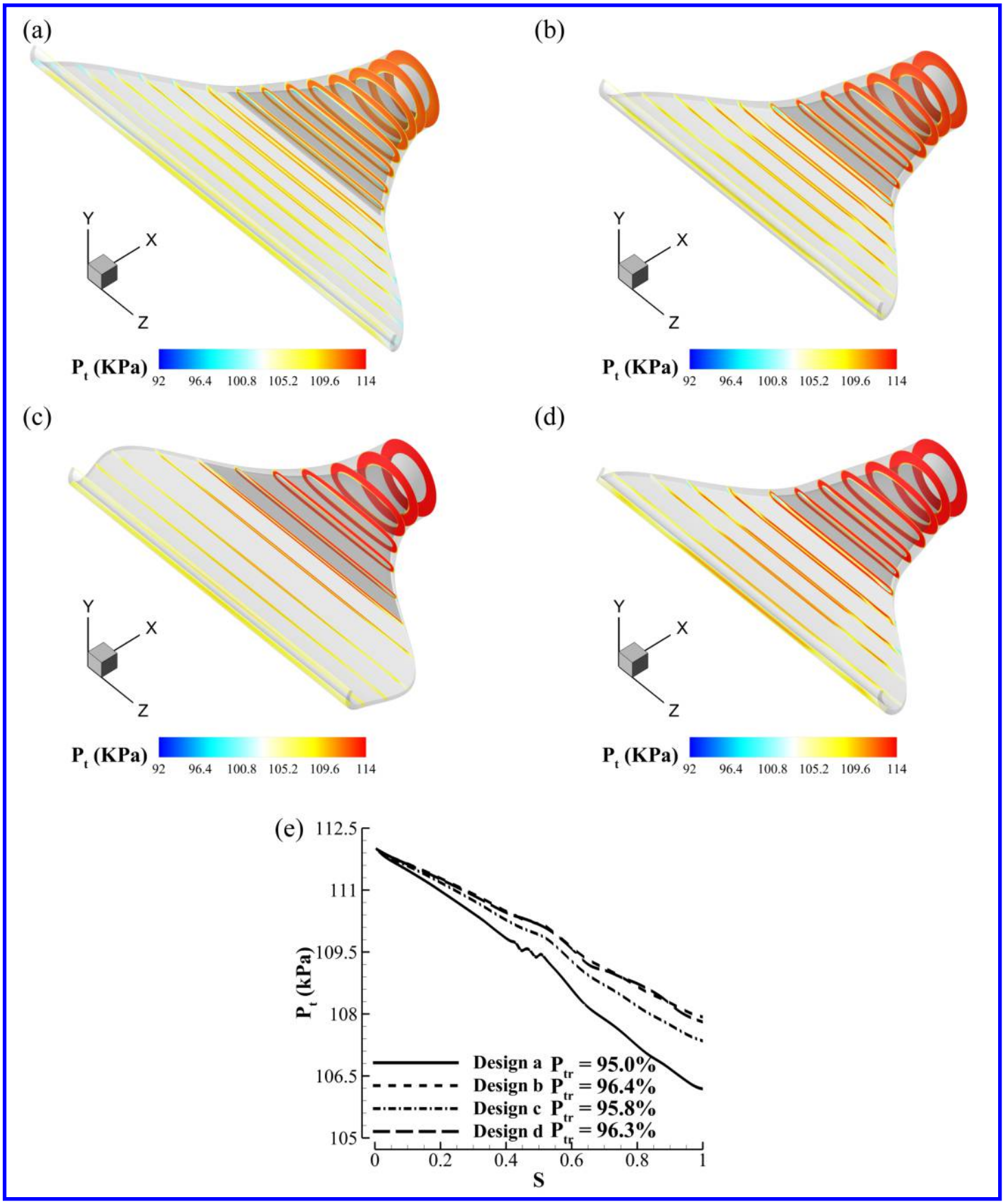

Figure 8: 2D flow slices along the streamwise direction. Colored by total pressure. (a) Design a; (b) design b; (c) design c; (d) design d; (e) the corresponding mass flow averaged total pressure distribution along the stream wise direction.

At last, we measure the flow deviation angle β at the injection duct outlet, and the results is plotted in Fig. 9. We can see that lower W/D leads to much lower β angle. The maximum β angle decreases from 31° to 22° when the W/D drops from 6.5 to 5. Moreover, greater amplitude of duct diverging converging lead to smaller β angle distributions, but more easier to present separated flows (design c).

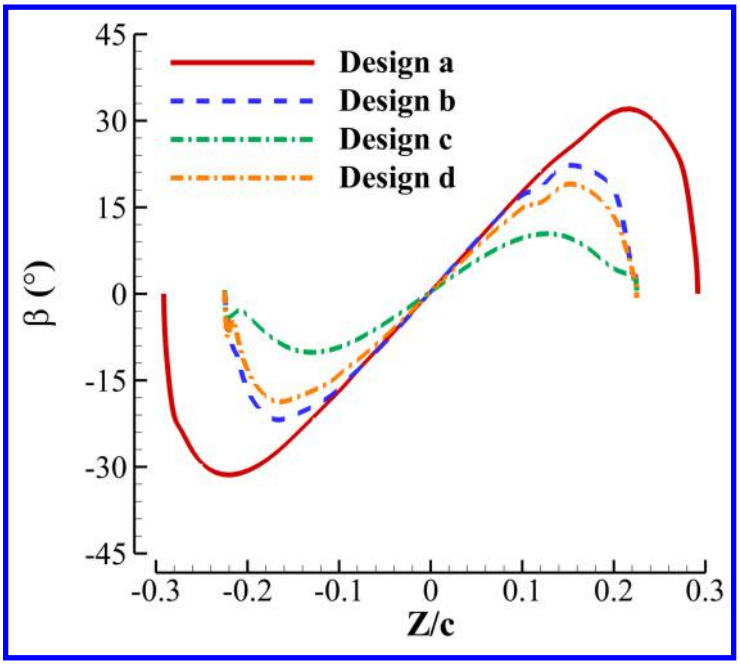

Figure 9: β angle distribution at the injeciotn duct outlet.

4 Conclusion

In the current work, four designs of injection duct span width distribution of co-flow jet (CFJ) flow control airfoils are presented. The aerodynamic performance of the injection ducts are evaluated via numerical simulations. The simulation results show that the duct span width distribution is crucial to control the spanwise velocity at the duct outlet. Smaller span over diameter ratio (W/D) leads to much smaller deviation angle (β) of the flow at the outlet. Moreover, a diverging-converging distribution of duct span width leads to even smaller β angle. However, such profiles are more likely to cause flow separation at the two ends of the duct in spanwise direction.

The duct with $W/D = 6.5$ (design a) shows 95% total pressure recovery, while the duct with $W/D = 5$ (design b) shows 96.4% total pressure recovery. The first duct with diverging-converging duct span width distribution (design c) presents only half of the maximum β angle comparing to design b, but the total pressure recovery is a little bit lower (95.8%) due to flow separation at the two ends of the duct in spanwise direction. The second duct with diverging-converging duct span width distribution (design d) presents 85% of the maximum β angle comparing to design b, and the total pressure recovery is almost the same (96.3%) since the flow separation at the two ends of the design c in spanwise direction are removed. The aerodynamic performance of design d is the best in terms of low spanwise velocity and high total pressure recovery,and it is expected to improve the aerodynamic performance of CFJ airfoil in cruise condition.

5 Acknowledgment

This project is sponsored by the Defense Advanced Research Projects Agency and monitored by the program manager Jean-Charles Ledé under Cooperative Agreement No.: HR0011-16-2-0052. The content of the information does not necessarily reflect the position or the policy of the Government, and no official endorsement should be inferred. The simulations are conducted on Pegasus supercomputing system at the Center for Computational Sciences at the University of Miami.

References

[1] G.-C. Zha and D. C. Paxton, "A Novel Flow Control Method for Airfoil Performance Enhancement Using Co-Flow Jet." *Applications of Circulation Control Technologies*, Chapter 10, p. 293-314, Vol. 214, Progress in Astronautics and Aeronautics, AIAA Book Series, Editors: Joslin, R. D. and Jones, G.S., 2006.

[2] G.-C. Zha, W. Gao, and C. Paxton, "Jet Effects on Co-Flow Jet Airfoil Performance," *AIAA Journal, No. 6,*, vol. 45, pp. 1222–1231, 2007.

[3] G.-C. Zha, C. Paxton, A. Conley, A. Wells, and B. Carroll, "Effect of Injection Slot Size on High Performance Co-Flow Jet Airfoil," *AIAA Journal of Aircraft*, vol. 43, 2006.

[4] G.-C. Zha, B. Carroll, C. Paxton, A. Conley, and A. Wells, "High Performance Airfoil with Co-Flow Jet Flow Control," *AIAA Journal*, vol. 45, 2007.

[5] Wang, B.-Y. and Haddoukessouni, B. and Levy, J. and Zha, G.-C., "Numerical Investigations of Injection Slot Size Effect on the Performance of Co-Flow Jet Airfoil," *Journal of Aircraft*, vol. Vol. 45, No. 6,, pp. pp.2084–2091, 2008.

[6] B. P. E. Dano, D. Kirk, and G.-C. Zha, "Experimental Investigation of Jet Mixing Mechanism of Co- Flow Jet Airfoil." AIAA-2010-4421, 5th AIAA Flow Control Conference, Chicago, IL, 28 Jun - 1 Jul 2010.

[7] B. P. E. Dano, G.-C. Zha, and M. Castillo, "Experimental Study of Co-Flow Jet Airfoil Performance Enhancement Using Micro Discreet Jets." AIAA Paper 2011-0941, 49th AIAA Aerospace Sciences Meeting, Orlando, FL, 4-7 January 2011.

[8] A. Lefebvre, B. Dano, W. Bartow, M. Fronzo, and G. Zha, "Performance and energy expenditure of coflow jet airfoil with variation of mach number," *Journal of Aircraft*, vol. 53, no. 6, pp. 1757–1767, 2016.

[9] A. Lefebvre, G-C. Zha, "Numerical Simulation of Pitching Airfoil Performance Enhancement Using Co-Flow Jet Flow Control," *AIAA paper 2013-2517*, June 2013.

[10] A. Lefebvre, G-C. Zha, "Cow-Flow Jet Airfoil Trade Study Part I : Energy Consumption and Aerodynamic Performance," *32nd AIAA Applied Aerodynamics Conference, AIAA AVIATION Forum, AIAA 2014-2682*, June 2014.

[11] A. Lefebvre, G-C. Zha, "Cow-Flow Jet Airfoil Trade Study Part II : Moment and Drag," *32nd AIAA Applied Aerodynamics Conference, AIAA AVIATION Forum, AIAA 2014-2683*, June 2014.

[12] J. R. Burley II, L. S. Bangert, and J. R. Carlson, "Static investigation of circular-to-rectangular transition ducts for high-aspect-ratio nonaxisymmetric nozzles." NASA Technical Paper 2534, 1986.

[13] W. H. Beyer, "Crc standard mathematical tables," *West Palm Beach, Fl.: Chemical Rubber Co., 1978, 25th ed., edited by Beyer, William H.*, 1978.

[14] Yang, Yunchao and Zha, Gecheng, "Super-Lift Coefficient of Active Flow Control Airfoil: What is the Limit?," *AIAA Paper 2017-1693, AIAA SCITECH2017, 55th AIAA Aerospace Science Meeting, Grapevine, Texas*, p. 1693, 9-13 January 2017.

[15] P. R. Spalart and S. R. Allmaras, "A one-equation turbulence model for aerodynamic flows," in *30th Aerospace Sciences Meeting and Exhibit, Aerospace Sciences Meetings, Reno, NV, USA, AIAA Paper 92-0439*, 1992.

[16] Y.-Q. Shen and G.-C. Zha, "Large Eddy Simulation Using a New Set of Sixth Order Schemes for Compressible Viscous Terms ," *Journal of Computational Physics*, vol. 229, pp. 8296–8312, 2010.

[17] Zha, G.C., Shen, Y.Q. and Wang, B.Y., "An improved low diffusion E-CUSP upwind scheme ," *Journal of Computer and Fluids*, vol. 48, pp. 214–220, Sep. 2011.

[18] Y.-Q. Shen and G.-Z. Zha , "Generalized finite compact difference scheme for shock/complex flowfield interaction," *Journal of Computational Physics*, vol. doi:10.1016/j.jcp.2011.01.039, 2011.

[19] Shen, Y.-Q. and Zha, G.-C. and Wang, B.-Y., " Improvement of Stability and Accuracy of Implicit WENO Scheme," *AIAA Journal*, vol. 47, No. 2, pp. 331–344, 2009.

[20] Shen, Y.-Q. and Zha, G.-C. and Chen, X.-Y., " High Order Conservative Differencing for Viscous Terms and the Application to Vortex-Induced Vibration Flows," *Journal of Computational Physics*, vol. 228(2), pp. 8283–8300, 2009.

[21] Shen, Y.-Q. and Zha, G.-C. , " Improvement of the WENO Scheme Smoothness Estimator," *International Journal for Numerical Methods in Fluids*, vol. DOI:10.1002/fld.2186, 2009.

[22] G.-C. Zha and E. Bilgen, "Numerical Study of Three-Dimensional Transonic Flows Using Unfactored Upwind-Relaxation Sweeping Algorithm," *Journal of Computational Physics*, vol. 125, pp. 425–433, 1996.

[23] B.-Y. Wang and G.-C. Zha, "A General Sub-Domain Boundary Mapping Procedure For Structured Grid CFD Parallel Computation," *AIAA Journal of Aerospace Computing, Information, and Communication*, vol. 5, No.11, pp. 2084–2091, 2008.

[24] Y.-Q. Shen, G.-C. Zha, and B.-Y. Wang, "Improvement of Stability and Accuracy of Implicit WENO Scheme ," *AIAA Journal*, vol. 47, pp. 331–344, 2009.

[25] PCA engineers, "Design of a mixed flow fan." Internal Report to University of Miami, 2017.